Photon emission and electron-positron photoproduction processes in the planar field of a bent single crystal

S. Bellucci
INFN-Laboratori Nazionali di Frascati, Via E. Fermi 40, 00044 Frascati, Italy

V. A. Maisheev
Institute for High Energy Physics, 142281, Protvino, Russia

(Received 30 July 2012; published 17 October 2012)

The process of photon emission by a high-energy electron or positron moving in a bent single crystal with a constant curvature is considered. The relations for differential energy losses of particles and polarization of emitted photons are obtained. Corrections due to multiphoton production are found. The comparison of calculations with existing experimental data is carried out. The process of photoproduction of electron-positron pairs in a bent single crystal is also studied. The differential probabilities of the process taking into account the photon polarization are presented. Equations are obtained which determine the variation of the Stokes parameters of γ quanta, and their solutions are given.

DOI: 10.1103/PhysRevA.86.042902 PACS number(s): 61.85.+p, 41.60.−m, 78.70.−g, 41.20.Jb

I. INTRODUCTION

In the recent years a number of experiments devoted to the interaction of ultrarelativistic particles with bent single crystals were performed [1–4]. In particular, the process of photon emission by electrons and positrons volume-reflected in planar electric fields of a bent silicon crystal was investigated [5,6]. The comparison of results of these measurements with the calculations [7] has shown satisfactory agreement between them. The calculations were carried out on the basis of the quasiclassical approach developed in Ref. [8]. This approach has a complicated enough mathematical form, and there are difficulties in the two-dimensional integration of strongly oscillating functions. Then, a simple method of calculation was proposed [9,10]. The method stands on the well-known theory of coherent bremsstrahlung in straight single crystals. Really, at large enough bending radii and on a short part of the trajectory, the radiation of a particle moving in a bent crystal is the same as in a straight one. The sum of such radiation energy losses from short parts should give the total energy losses from the whole of the trajectory. Despite the successful usage of the method [10] for simulations of the experiment [11], it is desirable to obtain a more rigorous consideration of the process. Apart from the rigor of treatment, such consideration can give limitations on the use of the method and describe the radiation process at small bending radii.

The present paper is devoted to provide a more evident and complete study of the radiation of over-barrier positrons and electrons moving in planar electric fields of bent single crystals. In a similar manner, another electromagnetic process (i.e., $e^{\pm}$ photoproduction) at similar conditions was also investigated. As a result, a detailed mathematical description of the processes was obtained, which is in agreement with the existing experimental data and may be used for calculations at various conditions. In addition, below we will compare our description with results of Refs. [12,13], in which the photon emission in bent single crystals was also considered. Below we will discuss the main results.

The attention to experiments with bent single crystals is motivated by new interesting possibilities for aims of collimation of accelerated beams in ring [Large Hadron Collider (LHC)] and [International Linear Collider (ILC)]. Additional feasible applications are pointed out in Ref. [7] (see also Refs. [14–17]).

The paper is organized as follows: In Sec. II we give a detailed description of photon emission by over-barrier charged particles in bent single crystals. In Sec. III we obtain differential probabilities of $e^{\pm}$ photoproduction in bent single crystals. Section IV is devoted to specific illustrations of investigated electromagnetic processes and Sec. V provides a discussion and a summary of the results.

II. RADIATION OF PARTICLES IN BENT SINGLE CRYSTALS

A. Motion in bent single crystals

One can describe the motion of ultrarelativistic particles in bent single crystals with the help of the following equations [18]:

$$E_0\beta^2 v_r^2/(2c^2) + U(r) + E_0\beta^2(R-r)/r = E = \text{const.}, \tag{1}$$

$$dy/dt = v_y = \text{const.}, \tag{2}$$

$$v_z = r\,d\phi/dt \approx c\left(1 - \frac{1}{2\gamma^2} - \frac{\left(v_r^2 + v_y^2\right)}{2c^2}\right). \tag{3}$$

These equations take place for the cylindrical coordinate system (r,ϕ,y). Here, v_r is the component of the particle velocity in the radial direction, v_y is the component of the velocity along the y axis, v_z is the tangential component of the velocity, R is the bending radius of a single crystal, E_0 and γ are the particle energy and its Lorentz factor, respectively, E is the constant value of the radial energy, $U(r)$ is the one-dimensional potential of a single crystal, c is the velocity of light, and β is the ratio of the particle velocity to the velocity of light. In this paper we consider the planar case, when the scattering is due to the interaction of particles with

the set of the crystallographic planes located normal to (r,ϕ) plane. In practice it means that $v_y/c \gg \theta_{ac}$ but $v_y/c \ll 1$ for ultrarelativistic particles, where θ_{ac} is the critical angle of axial channeling.

One can transform Eq. (1) into the following form:

$$E_0\beta^2 v_x^2/(2c^2) + U(x) + E_0\beta^2 x/R = E, \tag{4}$$

where x is the local Cartesian coordinate which is connected with the cylindrical coordinate r through the relation $x = R - r$ and $v_x = v_r$. We also changed the r value in the denominator of Eq. (1) on R. For a real experimental situation it brings a negligible mistake (of the order of x/R). In Eq. (4) the E value means the transversal energy.

The equations considered here describe the three-dimensional motion of particles in a bent single crystal in the cylindrical coordinate system. Let us introduce the Cartesian coordinate system in which the xy plane is coincident with the front edge of a single crystal. Now we can calculate x and y components of the velocity in this system:

$$V_x = \dot{X} = v_x \cos\phi + v_z \sin\phi \approx v_x + v_z\phi, \tag{5}$$

$$V_z = \dot{Z} = -v_x \sin\phi + v_z \cos\phi. \tag{6}$$

Figure 1 illustrates the geometry of proton beam volume reflection and different coordinate systems which will be used in our consideration.

Furthermore, we will study the ultrarelativistic case and put $\beta = 1$. From Eq. (4) we can get

$$\ddot{x} = -\frac{dU(x)}{dx}\frac{c^2}{E_0} - \frac{c^2}{R}. \tag{7}$$

Then, taking into account that $\phi \approx ct/R$, we obtain [from Eqs. (5)–(7)] for the transversal acceleration

$$\ddot{X} = \frac{c^2}{E_0} e\mathcal{E}(x(t)), \tag{8}$$

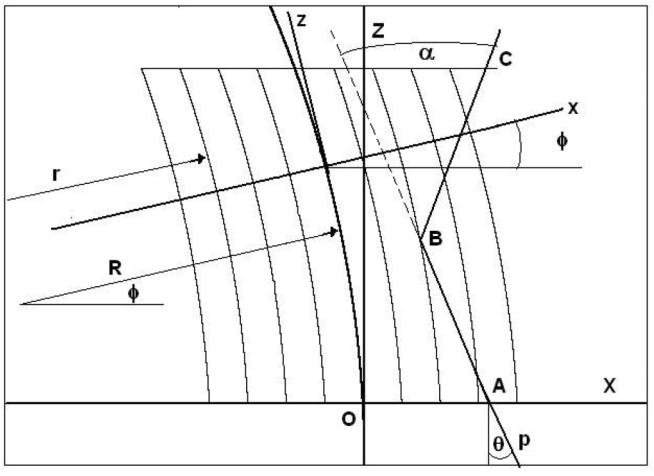

FIG. 1. Scheme of the volume reflection process. XYZ is the Cartesian coordinate system at the entrance in a single crystal, xyz is the local Cartesian coordinate system connected with the current location of a particle. The Y axis is directed normally to the plane of the figure. θ and α are the initial and volume reflection angles, respectively. AB and BC lines are the incoming and outgoing directions of a particle, respectively.

where e is the positive elementary charge and $\mathcal{E}$ is the interplanar electric field.

The effect of volume reflection takes place when particles with initial incoming angles larger than the critical channeling angle (over-barrier particles) have a tangency point with respect to the bent crystallographic planes inside the crystal volume. The critical point x_c (i.e., the point where the one-dimensional velocity is equal to zero) is determined by the equation

$$E - U(x_c) - E_0\beta^2 x_c/R = 0. \tag{9}$$

The process of volume reflection was studied in Ref. [18] (see also Ref. [19]). In particular, the angle of volume reflection as a function of the transversal energy has the form

$$\alpha_{vr}(E) = \frac{2c}{R} T(x_0,x_c), \tag{10}$$

where

$$T(x_0,x) = \int_{x_0}^{x} \left[\frac{1}{\sqrt{\frac{2c^2}{E_0\beta^2}[E - U(x) - E_0\beta^2 x/R]}} - \frac{1}{\sqrt{\frac{2c^2}{E_0\beta^2}[E - U(x_c) - E_0\beta^2 x/R]}} \right] dx. \tag{11}$$

This relation is written for the symmetric case of particle passage through a single crystal. In this case $|x_0 - x_c| \approx z_0^2/(8R)$, where z_0 is the thickness of a single crystal. In Ref. [18] it is also shown that the mean and mean square angles of volume reflection follow from the equations

$$\langle\alpha_{vr}\rangle = \frac{1}{\delta E}\int_E^{E+\delta E} \alpha_{vr}(E)dE, \tag{12}$$

$$\sigma_{vr}^2 = \frac{1}{\delta E}\int_E^{E+\delta E} [\alpha_{vr}(E) - \langle\alpha_{vr}\rangle]^2 dE. \tag{13}$$

It is easy to understand [due to the periodicity of $U(x)$] that the angle $\alpha_{vr}(E)$ is a periodic function of the transversal energy with the period $\delta E = E_0\beta^2 d/R$. Note that the angle $\alpha_{vr}(E)$ is a periodic function of the initial coordinate x_0 and the square of the initial angle $\theta_0 = v_x(t=0)/c$. These periods are equal to d and $2d/R$, respectively.

From Eqs. (4) and (11) we can write (see also Ref. [18])

$$x - x_0 = \tilde{v}(x_0)[t - T(x_0,x)] - \frac{c^2}{2R}[t - T(x_0,x)]^2, \tag{14}$$

where

$$\tilde{v}(x_0) = c\sqrt{\theta_0^2 + 2[U(x_0) - U(x_c)]/(E_0\beta^2)} = c\theta_b \approx c\theta_0. \tag{15}$$

At $T(x_0,x) = 0$ Eq. (14) describes the free (noninteracting with the interplanar potential) motion of a particle. At the conditions $x \ll x_c$ and $x \gg x_c$, $T(x_0,x) \approx 0$ and $T(x_0,x) \approx \alpha_{vr}R/(2c)$, respectively. As was demonstrated in Ref. [18], a noticeable variation of the $T(x_0,x)$ value takes place in the

vicinity of the x_c point. Our calculations show that, due to the $T(x_0,x)$ term, the coordinate x undergoes weak vibrations at the motion of particles. From here we obtain the equation for x averaged over these vibrations:

$$x = x_0 + \tilde{v}_0(x_0)t - c^2t^2/(2R) \text{ if } t \leqslant t_c, \tag{16}$$

$$x = x_0 + \tilde{v}_0\alpha_{vr}R/c - \alpha_{vr}^2R/2 + (\tilde{v}_0 - \alpha_{vr}c)t - c^2t^2/(2R) \text{ if } t > t_c, \tag{17}$$

$$t_c = \frac{R\tilde{v}_0}{c^2} - \frac{\alpha_{vr}R}{2c}. \tag{18}$$

The value $\dot{x}/c$ is the angle θ with respect to crystallographic planes, hence we can write

$$\theta = \frac{\tilde{v}_0}{c} - \frac{ct}{R} = \theta_b - \frac{ct}{R} \text{ if } t \leqslant t_c, \tag{19}$$

$$\theta = \frac{\tilde{v}_0}{c} - \alpha_{vr} - \frac{ct}{R} = \theta_b - \alpha_{vr} - \frac{ct}{R} \text{ if } t > t_c. \tag{20}$$

From these equations it follows that x is a continuous function of time and the θ angle has a breaking at $t = t_c$.

B. Preliminary study of problem

It is well known that the process of radiation of a relativistic particle undergoing quasiperiodic motion may be characterized with the help of the parameter [8] $\rho = 2\gamma^2\langle[v(t) - v_m(t)]^2\rangle/c^2$, where $v(t)$, v_m are the current (as a function of time t) and mean transversal velocities of a particle, respectively, and the brackets $\langle\cdots\rangle$ denote averaging over time. The radiation process has a dipole (interference) character when $\rho \ll 1$ and a synchrotron-like character when $\rho \gg 1$. $\rho \sim 1$ is an intermediate case.

In the case of over-barrier motion ultrarelativistic particles intersect a set of parallel crystallographic planes and, because of this, their transversal velocities oscillate. The peculiarities of such a motion are the aperiodicity and amplitude variations of oscillations. However, on a short part of the particle trajectory these variations of period and amplitude are insignificant (for large enough bending radii). It allows us to calculate the ρ parameter for every oscillation. These calculations [for 120 GeV positrons moving in the (110) silicon plane] show that the ρ parameter is smaller than 2 and exceeds 1 only for several oscillations in the vicinity of a critical point. At the decreasing of the particle energy the maximal value of ρ slowly decreases. Furthermore, we suggest that the radiation process has a dipole character. For estimating the ρ parameter one can use the equation

$$\rho \approx \frac{\langle U^2(x)\rangle - \langle U(x)\rangle^2}{2m^2c^4\left[\theta_c^2 + 2(x_0 - x)/R\right]}. \tag{21}$$

where $\langle U(x)\rangle$ and $\langle U^2(x)\rangle$ are the mean and mean square of the planar potential, respectively. This relation is violated in the region close to the critical point; in this region, in fact, a more exact calculation yields a result larger by about a factor of two. Note that $\langle U^2(x)\rangle - \langle U(x)\rangle^2 = 42.3$ eV^2 for the silicon (110) plane.

In the case of dipole photon emission the equation for calculation of energy losses has the form Ref. [20]

$$d\mathcal{E}_\gamma = \frac{e^2\omega_\gamma d\omega_\gamma}{4\pi c^3}\int_\delta^\infty \frac{d\omega}{\omega^2}\left[\frac{E_0^2 + E'^2}{E_0E'} - \frac{4\delta}{\omega}\left(1 - \frac{\delta}{\omega}\right)\right] \times |\ddot{X}(\omega)|^2, \tag{22}$$

$$\delta = \frac{\omega_\gamma m^2c^4}{2E_0E'}, \quad \ddot{X}(\omega) = \int_{-\infty}^{\infty}\ddot{X}(t)e^{i\omega t}dt, \tag{23}$$

where m is the particle mass, ω_γ is the photon frequency, and E' is the particle energy after emission.

Thus, we see that the Fourier components of the acceleration [see Eq. (8)] should be found. For this aim, it is convenient to present the interplanar electric field as a Fourier series over reciprocal vectors of a crystallographic structure [21]:

$$\mathcal{E}(x) = \frac{i8\pi^2e\tilde{Z}}{\Delta d}\sum_{N=-\infty}^{\infty}U(N)N\exp(-iN2\pi x/d), \tag{24}$$

where $\tilde{Z}e$ is the nuclear charge, d is the interplanar distance, Δ is the volume of the fundamental cell of the structure, and

$$U(N) = S(\mathbf{g})\frac{1 - F(g)}{g^2}\exp(-Ag^2/2), \tag{25}$$

where F is the atomic form factor, S is the structure factor, A is the mean square radius of thermal atomic vibrations, and g is the reciprocal vector of the crystallographic lattice. For a structure with the cubic fundamental cell $\mathbf{g} = \frac{2\pi}{a}(N_1\mathbf{i} + N_2\mathbf{j} + N_3\mathbf{k})$, with $\mathbf{i}$, $\mathbf{j}$, and $\mathbf{k}$ unit vectors directed along the main sides of cube. The interplanar distance for the plane defined by the Miller indices (k_1,k_2,k_3) reads

$$d = \frac{a}{N_s\sqrt{k_1^2 + k_2^2 + k_3^2}}, \tag{26}$$

where the numbers N_1, N_2, N_3 are equal to $N_1 = Nk_1$, $N_2 = Nk_2$, $N_3 = Nk_3$, and N_s is the smallest positive number which satisfies the condition $S(g(N_sk_1,N_sk_2,N_sk_3)) \neq 0$. Thus, we get $g = GN$, $G = 2\pi/d$.

Now we transform this relation in the following form, which is more convenient for calculations:

$$\mathcal{E}(x) = \frac{i8\pi^2e\tilde{Z}}{\Delta d}\sum_{N=1}^{\infty}U(N)N[\exp(iNGx) - \exp(-iNGx)]. \tag{27}$$

Such a representation has positive as well as negative sides. The negative one is the loss of correspondence, when every term corresponds to one vector of the reciprocal space, the positive one includes the possibility of a more compact writing of results, and other advantages.

Then, we find the Fourier components of the transversal acceleration

$$\ddot{X}_\omega = \int_0^{t_c} \ddot{x}(t) \exp i\omega t = \frac{i(16\pi^2)e^2\tilde{Z}}{\Delta d} \sum_{N=1}^{\infty} U(N) N J(N,\omega), \tag{28}$$

$$\ddot{X}_\omega \ddot{X}^*_\omega = \frac{\tilde{Z}^2 e^4 64\pi^4}{m^2\gamma^2\Delta^2 d^2} \sum_{N=1}^{\infty} N^2 U^2(N) J(N) J^*(N) + \sum_{N=1}^{\infty} \sum_{M=1,\neq N}^{\infty} NMU(N)U(M)J(N)J^*(M), \tag{29}$$

where

$$J(N,\omega) = \int_0^{t_c} (\exp\{iNG[v_0(x_0)t - c^2t^2/(2R)]\} - \exp\{-iNG[v_0(x_0)t - c^2t^2/(2R)]\}) e^{i\omega t} dt. \tag{30}$$

Here we take the $x(t)$ function from Eqs. (16) and (17). With the help of the relation $Y = \theta_b - \theta$ [see Eqs. (19) and (20)] we get

$$J(N) = \frac{R}{c} \int_0^{\theta_b - \theta_c} \{\exp[iNG(\theta_b Y R - RY^2/2)] - \exp[-iNG(\theta_b Y R - RY^2/2)]\} e^{\frac{iRY\omega}{c}} dY. \tag{31}$$

Here, terms like $\exp iNGx_0$, were omitted because they do not give a contribution in the result. These components were calculated for the period of time from 0 to t_c. The case when $t > t_c$ will be considered below. Then we represent $J(N, N > 0) = I_1(N) + I_2(N)$, where

$$I_1(N) = \sqrt{\frac{2R}{NGc^2}} \exp\left(-iRC_1^2\right) \int_{Z_0}^{Z_1} \exp(iZ^2) dZ, \tag{32}$$

$$Z_0 = \sqrt{\frac{R}{2NG}} \left(\frac{\omega}{c} - NG\theta_b\right), \tag{33}$$

$$Z_1 = \sqrt{\frac{R}{2NG}} \left(\frac{\omega}{c} - NG\theta_c\right), \tag{34}$$

$$C_1 = \sqrt{\frac{2}{NG}} \left(\frac{\omega}{c} - NG\theta_b\right), \tag{35}$$

$$I_2(N) = \sqrt{\frac{2R}{NGc^2}} \exp\left(iRC_2^2\right) \int_{Z_2}^{Z_3} \exp(-iZ^2) dZ, \tag{36}$$

$$Z_2 = -\sqrt{\frac{R}{2NG}} \left(\frac{\omega}{c} + NG\theta_b\right), \tag{37}$$

$$Z_3 = -\sqrt{\frac{R}{2NG}} \left(\frac{\omega}{c} + NG\theta_c\right), \tag{38}$$

$$C_2 = \sqrt{\frac{2}{NG}} \left(\frac{\omega}{c} + NG\theta_b\right). \tag{39}$$

Then, we get

$$I_1(N) I_1^*(N) = \frac{dR}{\pi N c^2} \left[\mathcal{F}_C^2(Z_0, Z_1) + \mathcal{F}_S^2(Z_0, Z_1)\right], \tag{40}$$

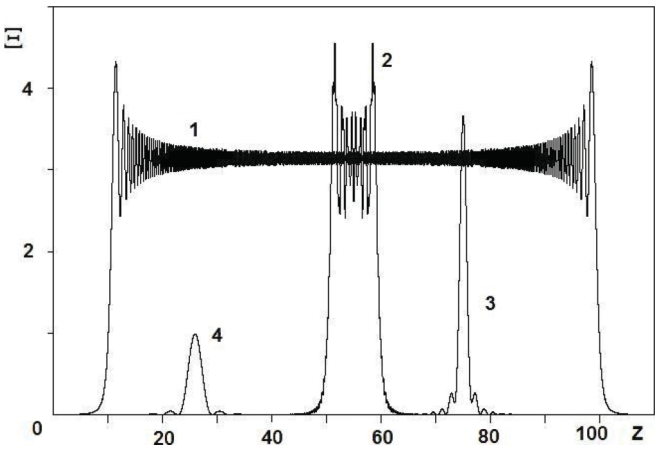

FIG. 2. Curves 1–4 illustrate $\Xi(Z)$ function at $A = 100, 60, 76, 25.5$ and $B = 10, 50, 74, 26.5$, respectively. For better presentation, curves 3 and 4 were shifted.

where $\mathcal{F}_C(Z_0, Z_1) = \int_{Z_0}^{Z_1} \cos(Z^2) dZ$ and $\mathcal{F}_S(Z_0, Z_1) = \int_{Z_0}^{Z_1} \sin(Z^2) dZ$. For $I_2(N) I_2^*(N)$ we obtain a similar expression.

Let us consider the expression $\Xi(Z) = \mathcal{F}_C^2(Z_0, Z_1) + \mathcal{F}_S^2(Z_0, Z_1)$ at $Z_0 = Z - A$, $Z_1 = Z - B$ as a function of the Z variable. We see in Fig. 2 that, at the condition $|A - B| \gg 1$, $\Xi(Z)$ is an oscillating function (around the ordinate equal to π) in the range from B to A. Outside this region the function is close to zero.

Let us assume for simplicity that $\theta_b > \theta_c > 0$. Then, $[I_1(N) + I_2(N)][I_1^*(N) + I_2^*(N)] \approx I_1(N) I_1^*(N)$. This conclusion follows from the corresponding behavior of the Ξ functions. One can see that the frequency interval which brings the main contribution is $\frac{\omega}{c} \approx 2\pi N\theta_c/d - 2\pi N\theta_b/d$. The terms in the double sum of Eq. (29) have the following form:

$$J(N)J^*(M) + J^*(N)J(M) = \frac{2dR}{\pi c^2 \sqrt{NM}} \{\cos\varphi[\mathcal{F}_C(N)\mathcal{F}_C(M) + \mathcal{F}_S(N)\mathcal{F}_S(M)] + \sin\varphi[\mathcal{F}_C(N)\mathcal{F}_S(M) - \mathcal{F}_S(N)\mathcal{F}_C(M)]\}, \tag{41}$$

where angle

$$\varphi = R\left[C_1^2(M) - C_1^2(N)\right] = \frac{Rd}{4\pi}\left(\frac{1}{M} - \frac{1}{N}\right)\frac{\omega^2}{c^2} + \frac{\pi R}{d}(M - N)\theta_b^2. \tag{42}$$

In these equations the $\mathcal{F}_C$ and $\mathcal{F}_S$ functions have the same arguments Z_0 and Z_1 (they are omitted) but they differ by the indices N and M. From Eq. (41) one can see that the result is a strongly oscillating function of ω (due to $\cos\varphi$ and $\sin\varphi$ multipliers). Below we will show that these terms give results close to zero.

It should be noted that, for brevity, we use in the equations throughout the paper the notation $U^2(N)$. However, for the case of a complex structure factors, $U(N)U^*(N)$ should be used instead of U^2.

C. General equations

Now we can write the final equation for radiation energy losses

$$d\mathcal{E}_\gamma = \frac{8\pi n\sigma_0 R^2\delta^2 dE_\gamma}{c^2 N_a \Delta}\left\{[1+(1-x)^2]\psi_1 - \frac{2}{3}(1-x)\psi_2\right\}, \tag{43}$$

where $x = E_\gamma/E_0$, E_γ is the energy of the emitted photon with the frequency ω_γ, $n = N_a/\Delta$ is the atomic density of a single crystal with N_a atoms in its fundamental cell, $\sigma_0 = \alpha_{\rm QED}\tilde{Z}^2 r_e^2$ is the characteristic cross section and $\alpha_{\rm QED}$ is the fine structure constant, $r_e = e^2/(mc^2)$. In this equation the coefficient $2/3$ was introduced for comparison with the standard theory in straight single crystals. The other functions are defined by the following equations:

$$\psi_1 = \sum_{N=1}^{\infty} U^2(N)\Phi_1(N), \quad \psi_2 = \sum_{N=1}^{\infty} U^2(N)\Phi_2(N), \tag{44}$$

where

$$\Phi_1(N) = \int_1^\infty \frac{\Psi(w,N)dw}{w^2}, \tag{45}$$

$$\Phi_2(N) = 6\int_1^\infty \left(\frac{1}{w^3} - \frac{1}{w^4}\right)\Psi(w,N)dw, \tag{46}$$

$$\Psi(w,N) = \left[\mathcal{F}_C^2\left(w - \frac{NG\theta_b c}{\delta}, w - \frac{NG\theta_c c}{\delta}\right) + \mathcal{F}_S^2\left(w - \frac{NG\theta_b c}{\delta}, w - \frac{NG\theta_c c}{\delta}\right)\right], \tag{47}$$

where

$$\mathcal{F}_C\left(w - \frac{NG\theta_b c}{\delta}, w - \frac{NG\theta_c c}{\delta}\right) = \int_{w-\frac{NG\theta_b c}{\delta}}^{w-\frac{NG\theta_c c}{\delta}} \cos(W_{\rm min}Z)^2 dZ, \tag{48}$$

$$\mathcal{F}_S\left(w - \frac{NG\theta_b c}{\delta}, w - \frac{NG\theta_c c}{\delta}\right) = \int_{w-\frac{NG\theta_b c}{\delta}}^{w-\frac{NG\theta_c c}{\delta}} \sin(W_{\rm min}Z)^2 dZ, \tag{49}$$

Here we introduced the variable $w = \omega/\delta$ and the value $W_{\rm min} = \frac{1}{2}\sqrt{\frac{Rd}{\pi N}}\delta/c$.

The contribution of the sum with terms containing $U(N)U(M)$ values with different N and M numbers [see Eq. (29)] in the total differential energy loss is close to zero. Let us consider the terms defined by Eqs. (41) and (42). We should make the change $\omega = w\delta$ and then we find the period of variation of the function $\varphi(w^2)$ in Eq. (42). The order of magnitude of this period is approximately $T_w \sim 32\pi^2[\lambda_c^2/(dR)](E_0^2/E_\gamma^2)$. One can see that, due to the factor $\lambda_c^2/(dR)$, we have for the period $T_w \ll 1$. It means that integrals of the type $\int_1^\infty \sin\varphi f(w)dw$ [where $f(w)$ is a weakly varied function, such as, for example, $f(w) = 1/w^2$; see Eq. (45)] are approximately equal to zero.

Besides, the angle of volume reflection is a function of the transversal energy. Because of this, the averaging over the period of the result [see Eq. (43)] for the transversal energy is also needed. Then we get

$$\left\langle\frac{d\mathcal{E}_\gamma}{dE_\gamma}\right\rangle = \frac{1}{\delta E}\int_E^{E+\delta E}\frac{d\mathcal{E}_\gamma(\alpha_{vr})}{dE_\gamma}dE. \tag{50}$$

However, the angle of volume reflection depends weakly on the transversal energy, for large enough bending radii. Hence, in this case there is no necessity for the averaging.

Now we can consider the case when $t > t_c$ or, in other words, when the particle crosses the area where the critical point is located. In this case, the resulting differential losses are the sum of losses from $t = 0$ to t_c and from t_c to t_e. Interferences between these regions are practically absent, as it is easy to show by a direct calculation of the values $J(N,t<t_c)J^*(N,t>t_c) + J^*(N,t<t_c)J(N,t>t_c)$.

The case when $t < t_c$ is obvious: instead of the angle θ_c the angle $\theta < \theta_c$ should be used, according to Eq. (19).

D. Approximation equations

In the range of variation of the w variable between $NG\theta_b c/\delta$ and $NG\theta_c c/\delta$, the function $\Psi(w,N)$ is approximately constant, at the condition

$$\kappa = \sqrt{\frac{\pi RN}{d}}(\theta_b - \theta_c) \gg 1. \tag{51}$$

This constant is equal to $\pi/W_{\rm min}^2$. Then, taking the integrals in Eqs. (45) and (46) we get the approximate relation for differential energy losses of the particle:

$$d\mathcal{E}_\gamma = \frac{16\pi^2 n\sigma_0 R\delta dE_\gamma}{c\Delta N_a}\left\{[1+(1-x)^2]\tilde{\psi}_1 - \frac{2}{3}(1-x)\tilde{\psi}_2\right\}, \tag{52}$$

$$\tilde{\psi}_1 = \sum_{N=1}^{\infty} U^2(N)\left(\frac{1}{\theta_{\rm min}} - \frac{1}{\theta_b}\right)\eta\left(\theta_b - \frac{\delta}{NGc}\right), \tag{53}$$

$$\tilde{\psi}_2 = 6\sum_{N=1}^{\infty} U^2(N)\left[\frac{\delta}{2(NGc)}\left(\frac{1}{\theta_{\rm min}^2} - \frac{1}{\theta_b^2}\right) - \frac{\delta^2}{3(NGc)^2}\left(\frac{1}{\theta_{\rm min}^3} - \frac{1}{\theta_b^3}\right)\right]\eta\left(\theta_b - \frac{\delta}{NGc}\right). \tag{54}$$

Here, $\eta(x)$ is the step function [$\eta(x) = 0$ if $x < 0$ and $\eta(x) = 1$ if $x > 0$], $\theta_{\rm min}(N,\omega) = \delta/(NGc)$ if $N \leqslant N_F$ and $= \theta_c$ if $N > N_F$, where N_F is the integer part of the value $d\delta/(2\pi c\theta_c)$.

In the report [10] coherent radiation in bent single crystals was considered. This consideration was based on the intuitive idea that, at large enough bending radii, the radiation process on a short distance of the particle trajectory is close to the radiation process in straight single crystals. Mathematically, this idea reads

$$\frac{d\mathcal{E}_\gamma}{dE_q}(E_q) = R\int_{\theta_1}^{-\theta_{\rm min}}\frac{dI}{dE_q}(\tilde{\theta})d\tilde{\theta} + R\int_{\theta_{\rm min}}^{\theta_2}\frac{dI}{dE_q}(\tilde{\theta})d\tilde{\theta}, \tag{55}$$

where $\theta_1 < -\theta_{\rm min}$ and $\theta_2 > \theta_{\rm min}$ are the entrance and exit angles, respectively. In the case when $t_2 < t_c$ ($t_1 > t_c$), one plain integral should be used. Here, $dI(\theta)/dE_q$ is the well-known intensity of coherent bremsstrahlung (in the straight crystals) [8,22–24]. Equation (52) may be applied for calculations of

the energy losses in a straight single crystal, if one replaces the bending radius R by the crystal thickness z_0 and takes the following $\tilde{\psi}_1$ and $\tilde{\psi}$ functions:

$$\tilde{\psi}_1 = \sum_{N=1}^{\infty} \frac{U^2(NG)}{\theta^2}\eta\left(\theta - \frac{\delta}{NGc}\right),$$
$$\tilde{\psi}_2 = 6\sum_{N=1}^{\infty} \frac{U^2(NG)\delta}{NGc}\left(\frac{1}{\theta^3} - \frac{\delta}{NGc\theta^4}\right)\eta\left(\theta - \frac{\delta}{NGc}\right), \tag{56}$$

where θ is a constant angle relative to the plane. If we substitute this intensity (the energy losses divided by z_0) into Eq. (55) and take the integrals then we get Eqs. (52)–(54). Thus, the above-mentioned intuitive idea is true and Eq. (51) reflects the condition of validity for such a consideration. Our specific calculations (see below) also support this approach. From this fact, some important conclusions follow:

(1) At the coherent radiation process, a particle transfers to a single crystal discrete quantities of momentum which are equal to $\hbar GN$.

(2) Coherent radiation in a bent crystal is accompanied by incoherent photon emission which is approximately as in a straight one; the total differential energy losses are equal to

$$d\mathcal{E}_\gamma^T = d\mathcal{E}_\gamma^C + d\mathcal{E}_\gamma^A, \tag{57}$$

where the first term on the right-hand side is a coherent contribution [see Eq. (52)] and the second term is an incoherent one.

(3) The polarization of the radiation in a bent crystal on a short distance is approximately the same as in a straight one and it is defined by the angle θ. One can write for the total linear polarization $\mathcal{P}$ of the radiation

$$\mathcal{P}(x)d\mathcal{E}_\gamma^T = \frac{16\pi^2 n\sigma_0 R\delta d E_\gamma}{c\Delta N_a}2(1-x)\tilde{\psi}_3, \tag{58}$$

where

$$\tilde{\psi}_3 = \sum_{N=1}^{\infty} U^2(N)\frac{\delta}{3(GNc)}\left(\frac{1}{\theta_{\min}^3} - \frac{1}{\theta_b^3}\right)\eta\left(\theta_b - \frac{\delta}{GNc}\right). \tag{59}$$

Here we did not multiply numerical coefficients for comparison with corresponding relations in a straight crystals.

E. Total characteristics

In this section we present the total (integrated over the energy) characteristics of the radiation process. They are calculated only for the coherent part of the process.

The total coherent cross section of photon emission in a straight single crystal is equal to

$$\sigma_c = \frac{\sigma_0 B u^2 G^2 E_0 \lambda_c}{4mc^2}\sum_{N=1}^{\infty} U^2(N)\Phi(u/N), \tag{60}$$

where $u = 2mc^2/(GE_0\theta\lambda_c)$, $B = 16\pi^2/(N_a\Delta)$, $\lambda_c = \hbar/(mc)$, and the function $\Phi(x)$ is defined by the equation

$$\Phi(x) = \left(\frac{1}{2} - \frac{x}{2} - \frac{x^2}{4}\right)\ln\left(1+\frac{4}{x}\right) + \frac{2+2x-x^3/8}{x+4} + \frac{x}{2} + \frac{x^2}{8} - \frac{4}{(x+4)^2}. \tag{61}$$

The integral of the cross section over the angle θ has the form

$$\int_{\theta_1}^{\theta_2}\sigma_c(\theta)d\theta = \frac{\sigma_0 BG}{2}\sum_{N=1}^{\infty} U^2(N)N|\Phi_1(u_1/N) - \Phi_1(u_2/N)|, \tag{62}$$

where $u_1 = 2mc^2/(GE_0\theta_1\lambda_c)$ and $u_2 = 2mc^2/(GE_0\theta_2\lambda_c)$ and function $\Phi_1(x)$ is

$$\Phi_1(x) = \frac{x^2}{2} + \frac{4}{4+x} + \frac{5}{3}(x+4) - \frac{(x+4)^2}{6} + 2\ln\left(x+\frac{x^2}{4}\right) + \left(\frac{x+4}{2} - \frac{x^2}{4} - \frac{x^3}{12}\right) \times \ln\left(1+\frac{4}{x}\right) - \frac{4}{3}\ln\left(1+\frac{x}{4}\right). \tag{63}$$

Note that for correct usage of this equation the angles θ_1 and θ_2 should be of the same sign. At $\theta = 0$ the cross section tends to infinity. Besides, $dz \approx cdt \approx Rd\theta$. The total coherent probability to emit one photon on a thickness z_0 ($z_0 = R|\theta_2 - \theta_1|$) is equal to $nR\int_{\theta_1}^{\theta_2}\sigma_c(\theta)d\theta$. This relation is valid at small enough z_0 (see below).

The total coherent intensity of radiation in a straight single crystal is

$$\mathcal{I} = \frac{\sigma_0 n B u^2 G^2 E_0^2 \lambda_c}{4mc^2}\sum_{N=1}^{\infty} U^2(N)\xi(u/N), \tag{64}$$

where

$$\xi(x) = \frac{1}{4+x}(-2+2x+x^2) + \ln\left(1+\frac{4}{x}\right)\left(\frac{1}{2} - \frac{x}{2} - \frac{3x^2}{8}\right) + \frac{(2+x)^2}{(4+x)^2} + \frac{x}{2} - \frac{32}{3(4+x)^3}. \tag{65}$$

The integral of intensity over the angle θ has the form

$$\int_{\theta_1}^{\theta_2}\mathcal{I}(\theta)d\theta = \frac{\sigma_0 nBGE_0}{2}\sum_{N=1}^{\infty} U^2(N)N|\xi_1(u_1/N) - \xi_1(u_2/N)|, \tag{66}$$

$$\xi_1(x) = \frac{x^2}{2} - \frac{4}{4+x} - \frac{x}{8}(-4+2x+x^2)\ln\frac{4+x}{x} + \frac{16}{3(4+x)^2}. \tag{67}$$

The total coherent energy losses in a bent single crystal are $\mathcal{E}_\gamma^C = R\int_{\theta_1}^{\theta_2}\mathcal{I}(\theta)d\theta$.

F. Taking into account multiphoton production

In order to take into account the multiphoton production from a single particle, we employ the correspondence between

electromagnetic processes in bent and nonbent single crystals. The emission process of a single photon can be described by the following equation:

$$\frac{dN_e}{N_e} = -n\sigma_\gamma(\epsilon,E_0,z)dz, \tag{68}$$

where $N_e(z)$ is the flux of electrons (positrons) which emitted one photon on a thickness from $z=0$ up to z, and $\sigma_\gamma(\epsilon,E_0,z)$ is the cross section of coherent bremsstrahlung on the current coordinate $z=ct$ of a crystal. This cross section has a form $\sigma_\gamma(\epsilon,E_0,z)=\int_\epsilon^{E_0}\frac{d\sigma_\gamma(E_0,z)}{dE_\gamma}dE_\gamma$ and takes into account the radiation of photons in the energy range from ϵ up to E_0. The value $n\sigma_\gamma(\epsilon,E_0,z)dz$ is the probability for an electron to emit one photon in the thickness dz in the energy range from ϵ up to E_0. It is connected with the intensity on the same coordinate [see Eq. (55)] by the relation $nd\sigma_\gamma/dE_\gamma=\frac{1}{E_\gamma}dI/dE_\gamma$. As was already shown, over a short distance dz we can take the required relations as in a straight single crystal. The necessity of introducing the minimal energy ϵ is as follows: The coherent bremsstrahlung cross section may be represented as the sum $d\sigma_\gamma=d\sigma_c+d\sigma_a$, where $d\sigma_c$ and $d\sigma_a$ are the coherent and incoherent parts of the process. The total coherent cross section σ_c is a finite value (if angle $\theta\neq 0$) and the incoherent cross section is similar to the analogous cross section in an amorphous medium, and at small photon energies it tends to infinity. Introducing the energy ϵ allows us to remove the low-energy part of radiation from our consideration, because these photons weakly influence the spectrum in the energy range of interest. By integration of Eq. (68) we obtain

$$N_e = N_0\left(1-\exp\left[-n\int_0^{z_0}\sigma(\epsilon,E_0,z)dz\right]\right), \tag{69}$$

where N_0 is the initial number of electrons and z_0 corresponds to a crystal thickness. Furthermore, we put $N_0=1$ or, in other words, our calculation will be done per one initial electron.

It is obvious that Eq. (69) is valid only for thin enough single crystals, when the probability of emission of two or more photons by one electron is small in comparison with 1. In this case our description of energy losses should be corrected.

The distribution of the photon radiation over the coordinate can be described by the following expression:

$$\frac{d^2N_e}{dzdE_+}(\epsilon,E_+,z) = \exp\left(-n\int_0^z\sigma_\gamma(\epsilon,E_0,z)dz\right) \times n\sigma_\gamma(\epsilon,E_0,z)\rho(\epsilon,E_0,E_+,z), \tag{70}$$

where the function

$$\rho(\epsilon,E_0,E_+,z)=\frac{1}{n\sigma_\gamma(\epsilon,E_0,z)}\frac{d\sigma_\gamma(\epsilon,E_0,E_+,z)}{dE_+}, \tag{71}$$

represents the normalized distribution over the energy of a secondary electron E_+ ($E_\gamma=E_0-E_+$).

Then we get

$$\frac{dN_{1e}}{dE_+}(\epsilon,E_+,z_0) = \int_0^{z_0}\frac{d^2N_e}{dzdE_+}(\epsilon,E_+,z) \times \exp\left(-n\int_z^{z_0}\sigma_\gamma(\epsilon,E_+,z)dz\right)dz, \tag{72}$$

$$\frac{dN_{2e}}{dE'}(\epsilon,E',z_0) = \int_0^{z_0}\int_{E'+\epsilon}^{E_0-\epsilon}\frac{d^2N_e}{dzdE_+}(\epsilon,E_+,z) \times\left\{1-\exp\left(-n\int_z^{z_0}\sigma_\gamma(\epsilon,E_+,z)dz\right)\right\} \times\rho(\epsilon,E_+,E',z)dE_+dz, \tag{73}$$

where E' is the energy of the electron which has energy E_+ before photon emission and the function $\rho(\epsilon,E_+,E',z)$ is similar to the case of Eq. (70). Here, N_1 is the number of electrons emitting one photon with energy $>\epsilon$ and N_2 is the number of electrons emitting two photons with energies $>\epsilon$. Now we can write, for the relation for radiation energy losses:

$$\frac{d\mathcal{E}}{dE'}(\epsilon,E',z_0) = (E_0-E')\left[\frac{dN_{1e}}{dE'}(\epsilon,E',z_0)+\frac{dN_{2e}}{dE'}(\epsilon,E',z_0)\right]. \tag{74}$$

For small thickness [when $n\int_z^{z_0}\sigma_\gamma(\epsilon,E',z)dz\ll 1$] Eq. (74) gives the result

$$\frac{d\mathcal{E}}{dE'}(\epsilon,E',z_0)=n(E_0-E')\int_0^{z_0}\frac{d\sigma_\gamma}{dE'}(\epsilon,E_0,E',z)dz. \tag{75}$$

At the condition $n\int_z^{z_0}\sigma_\gamma(\epsilon,E',z)dz\sim 1$ we should use Eqs. (72)–(74) for calculations. This consideration allows one to take into account (1) the nonlinear (exponential decrease) character of the process as a function of thickness and (2) the multiplicity of photon emission by one electron. Our consideration works for the case when no more than two high-energy photons may be emitted. Of course, it is easy to obtain the analogous relations for higher multiplicity, but there are difficulties of calculations of multidimensional integrals. The correct choice of ϵ cutting and other problems will be discussed below. Note that, in this section, for brevity of writing, we employ the integration over z. However, in reality, the integration over the angle θ is more suitable for calculations [see Eq. (55)].

III. $e^\pm$ PHOTOPRODUCTION IN BENT SINGLE CRYSTALS

A. Creation of $e^\pm$ pairs

In Ref. [8] a simple method was proposed which allows one to obtain the relations for the $e^\pm$-photoproduction process, provided the relations for photon emission by a positron (electron) are known. With the help of the method we get, for the differential probability of $e^\pm$ production by high-energy unpolarized photon moving in the planar electric field of a bent single crystal, the following relation:

$$\frac{d\mathcal{W}}{dy}=\frac{1}{2}\left(\frac{d\mathcal{W}_{||}}{dy}+\frac{d\mathcal{W}_\perp}{dy}\right) =\frac{8\pi n\sigma_0R^2\delta^2}{c^2N_a\Delta}\left\{[y^2+(1-y)^2]\psi_1+\frac{2}{3}y(1-y)\psi_2\right\}, \tag{76}$$

where $y=E_e/E_\gamma$ and E_γ is the photon energy, E_e is the energy of the positron or the electron, $\mathcal{W}_{||}$, $\mathcal{W}_\perp$ are the probabilities of photoproduction for a photon with the parallel and orthogonal linear polarizations relative to the

crystallographic plane. The ψ_1 and ψ_2 functions are defined by Eqs. (44)–(49) in which the δ value should be changed to the value

$$\delta = \frac{\omega_\gamma m^2 c^4}{2E_e(E_\gamma - E_e)}. \tag{77}$$

Here ω_γ is the photon frequency. The relations describing the motion of a photon in a bent single crystal was obtained in Ref. [25]. The variation of the angle θ (i.e., the direction of photon propagation relative to the crystallographic plane) is described by a relation similar to Eqs. (19) and (20). It means that we should take θ_b equal to the initial angle θ_0, and θ_c can reach the zero angle (breaking is absent). For the case when the entrance and exit angles have different sign, we should take the sum of the terms [see Eq. (55)].

In the case when $\kappa \gg 1$ [see Eq. (51)] these relations may be simplified:

$$\frac{d\mathcal{W}}{dy} = \frac{16\pi^2 n\sigma_0 R\delta}{c\Delta N_a}\left\{[y + (1-y)^2]\tilde{\psi}_1 + \frac{2}{3}y(1-y)\tilde{\psi}_2\right\}, \tag{78}$$

where the functions $\tilde{\psi}_1$ and $\tilde{\psi}_2$ have the form of Eqs. (53) and (54), with the corresponding value of δ [see Eq. (77)].

Now we can find the difference of differential probabilities:

$$\frac{1}{2}\left(\frac{d\mathcal{W}_{||}}{dy} - \frac{d\mathcal{W}_{\perp}}{dy}\right) = \frac{16\pi^2 n\sigma_0 R\delta}{c\Delta N_a} 2(1-x)\tilde{\psi}_3, \tag{79}$$

where the $\tilde{\psi}_3$ function is defined by Eq. (59).

Note that Eqs. (76) and (78) describe the coherent contribution in the process. The incoherent contribution is the same as in a straight single crystal.

B. Propagation of photons

Equations (76)–(79) are valid in thin crystals while $\mathcal{W}_{||}$, $\mathcal{W}_{\perp} \ll 1$. As known, the propagation of photons in a medium is determined by its permittivity tensor ε_{ij}, $i, j = 1$–3. For high-energy photons propagating in a straight single crystal, this tensor was found in Refs. [26,27]. The process is determined primarily by the transverse part of the permittivity tensor, while the longitudinal components of the tensor are higher-order infinitesimals in the interaction constant. The derivation of the tensor is based on the theory of coherent $e^{\pm}$ pair production [8,22]. Thus, we can employ these results for bent single crystals. It means that, on a short distance of the photon trajectory, the components of the tensor are functions of the θ angle. The correct description of the photon propagation in a medium includes equations for losses of photon flux and variations of Stokes parameters, which define a current polarization state of the beam. References [26,27] contain such a description for straight single crystals, when the components of the permittivity tensor are not changed along the photon trajectory. One can assume that the differential form Ref. [28] of these equations gives the description of the propagation process in bent single crystals. It should be noted that it is more convenient to employ the tensor $\eta_{\alpha\beta}(\alpha, \beta = 1, 2)$, which is the inverse tensor of ε_{ij}. Then we can write

$$\frac{c}{\omega_\gamma}\frac{dJ_\gamma}{dz} = -J_\gamma(-\mathcal{G} - \mathcal{F}\xi_1 - \mathcal{C}\xi_2 - \mathcal{B}\xi_3), \tag{80}$$

$$\frac{c}{\omega_\gamma}\frac{d\xi_1}{dz} = \mathcal{F}(1-\xi_1^2) - \mathcal{C}\xi_1\xi_2 - \mathcal{B}\xi_1\xi_3 - \mathcal{A}\xi_2 - \mathcal{D}\xi_3, \tag{81}$$

$$\frac{c}{\omega_\gamma}\frac{d\xi_2}{dz} = \mathcal{C}(1-\xi_2^2) - \mathcal{F}\xi_1\xi_2 - \mathcal{B}\xi_2\xi_3 + \mathcal{A}\xi_1 - \mathcal{E}\xi_3, \tag{82}$$

$$\frac{c}{\omega_\gamma}\frac{d\xi_3}{dz} = \mathcal{B}(1-\xi_3^2) - \mathcal{F}\xi_1\xi_3 - \mathcal{C}\xi_2\xi_3 + \mathcal{D}\xi_1 + \mathcal{E}\xi_2, \tag{83}$$

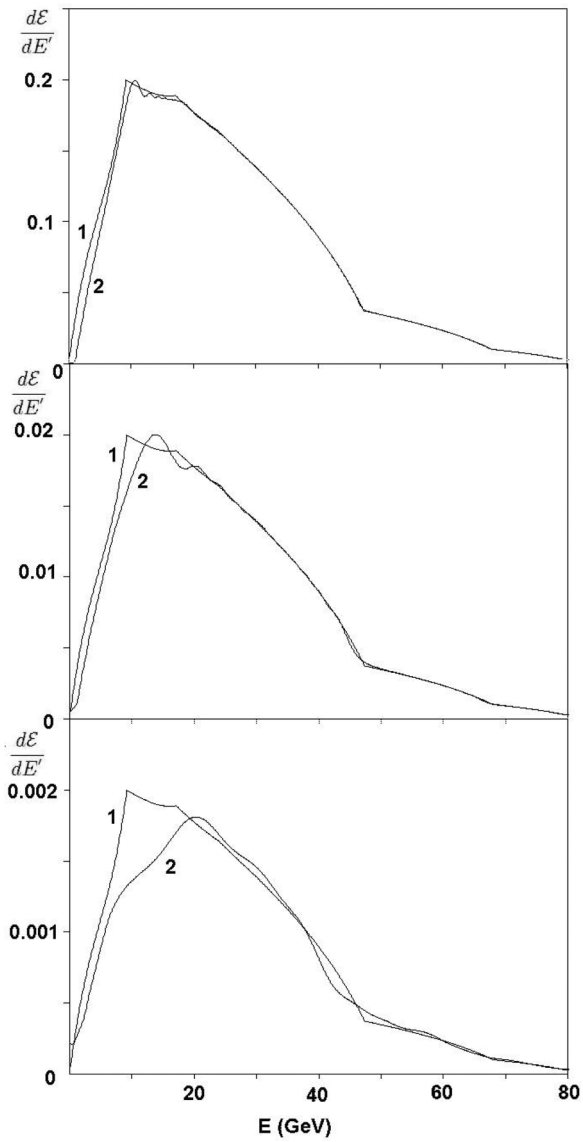

FIG. 3. Comparison of calculations of positron differential energy losses performed with the help of exact Eqs. (43)–(49) (curves 1) and approximated Eqs. (52)–(54) (curves 2). The conditions for calculations are $E_0 = 120$ GeV, $\theta_b = 110$ μrad, $\theta_c \approx 14$ μrad; the values of bending radii and κ are equal to 10 m and 40 (a), 1 m and 12.5 (b) and 0.1 m and 4 (c), respectively. The incoherent part of the losses is not presented.

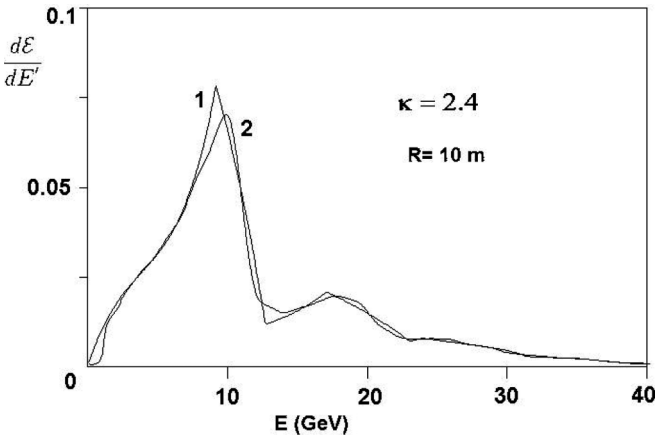

FIG. 4. Positron differential energy losses in a thin (0.06 mm) silicon single crystal performed with the help of Eqs. (43)–(49) (curve 1) and Eqs. (52)–(54) (curve 2). The incoherent part of the losses is not presented.

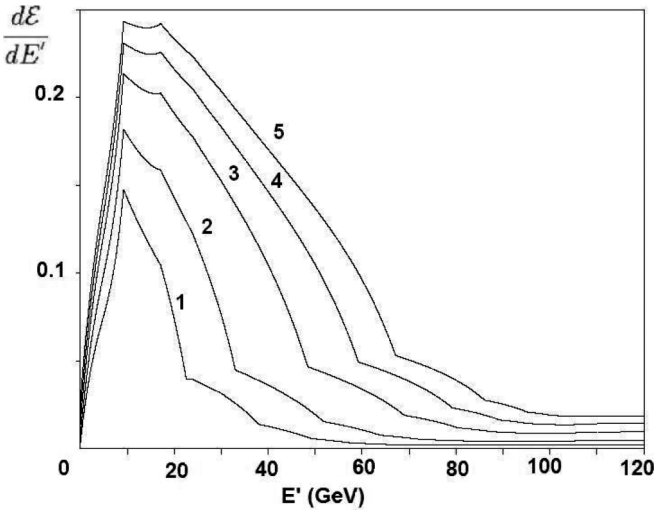

FIG. 5. Positron differential energy losses at different crystal thickness. The condition for calculations are $E_0 = 120$ GeV, $R = 10$ m. The curves 1–5 correspond to 0.25, 0.5, 1, 1,5, 2 mm of thickness (see text).

where

$$\mathcal{A}(z) = (\eta'_{11} - \eta'_{22})/2, \quad \mathcal{B}(z) = (\eta''_{11} - \eta''_{22})/2, \tag{84}$$

$$\mathcal{C}(z) = (\eta'_{12} - \eta'_{21})/2, \quad \mathcal{D}(z) = (\eta''_{12} - \eta''_{21})/2, \tag{85}$$

$$\mathcal{G}(z) = (\eta''_{11} + \eta''_{22})/2, \tag{86}$$

$$\mathcal{E}(z) = (\eta'_{12} + \eta'_{21})/2, \quad \mathcal{F}(z) = (\eta''_{12} + \eta''_{21})/2, \tag{87}$$

where $\eta_{\alpha\beta} = \eta'_{\alpha\beta} + i\eta''_{\alpha\beta}$. Besides, we assume that $|\eta_{\alpha\beta} - \delta_{\alpha\beta}| \ll 1$, where $\delta_{\alpha\beta}$ is the Kroneker δ function. Thus, the propagation process is described by the system of differential equations of the first order at the initial conditions $J(0) = 1$, $\xi_1(0) = \xi_{1,0}$, $\xi_2(0) = \xi_{2,0}$, $\xi_3(0) = \xi_{3,0}$. Note that $(-\mathcal{G} - \mathcal{F}\xi_1 - \mathcal{C}\xi_2 - \mathcal{B}\xi_3) \geqslant 0$ for any real medium.

Taking into account the possible expansion of the calculation method, we wrote equations in a more common form than is needed for the planar case of the crystal orientation. So, for the case under consideration $\mathcal{E} = 0$, $\mathcal{F} = 0$. Besides, $\mathcal{C} = 0$, $\mathcal{D} = 0$ if we choose the principal axes of the symmetric tensor along or parallel to the crystallographic plane.

The solution of the system has the following form:

$$J(z) = J(0)[\cosh b(z) + \xi_3(0)\sinh b(z)]e^{-w_0(z)}, \tag{88}$$

$$\xi_1(z) = \frac{\xi_1(0)\cos a(z) - \xi_2(0)\sin a(z)}{\cosh b(z) + \xi_3(0)\sinh b(z)}, \tag{89}$$

$$\xi_2(z) = \frac{\xi_1(0)\sin a(z) + \xi_2(0)\cos a(z)}{\cosh b(z) + \xi_3(0)\sinh b(z)}, \tag{90}$$

$$\xi_3(z) = \frac{\xi_3(0)\cosh b(z) + \sinh b(z)}{\xi_3(0)\sinh b(z) + \cosh b(z)}, \tag{91}$$

where

$$w_0(z) = \frac{\omega_\gamma}{2c}\int_0^z \mathcal{G}(z)dz = \mathcal{W}^T(z), \tag{92}$$

$$a(z) = \frac{\omega_\gamma}{c}\int_0^z \mathcal{A}(z)dz, \tag{93}$$

$$b(z) = \frac{\omega_\gamma}{c}\int_0^z \mathcal{B}(z)dz = \frac{1}{2}[\mathcal{W}_{||}(z) - \mathcal{W}_\perp(z)]. \tag{94}$$

Here $\mathcal{W}^T = \mathcal{W} + \mathcal{W}^A$, where $\mathcal{W}$ is defined by Eq. (78) and $\mathcal{W}^A$ is the incoherent contribution [25,26], $\mathcal{W}_{||}$, $\mathcal{W}_\perp$ are the same probabilities as in Eqs. (78) and (79). For the integration we should employ the following connection: $\theta = \theta_0 - z/R$ (for simplicity we put the initial angle $\theta > 0$). For completeness we write the following relations [26]:

$$\mathcal{A} = -\frac{Bn\sigma_0\lambda_c}{8\pi}\sum_{N=1}^{\infty} U^2(N)z_N^2 F_1'(z_N)(GN)^2, \tag{95}$$

where $z_N = 2mc^2/(E_\gamma GN\lambda_c\theta)$ and the F_1' function is

$$F_1{}'(z) = \begin{cases} \left[\sqrt{1-z} + \frac{z}{2}\ln\frac{1+\sqrt{1-z}}{1-\sqrt{1-z}}\right]^2 + \left[\sqrt{1+z} - \frac{z}{2}\ln\frac{\sqrt{1+z}+1}{\sqrt{1+z}-1}\right]^2 - \frac{\pi^2 z^2}{4}, & 0 < z \leqslant 1 \\ -\left[\sqrt{z-1} - z\arctan\frac{1}{\sqrt{z-1}}\right]^2 + \left[\sqrt{1+z} - \frac{z}{2}\ln\frac{\sqrt{1+z}+1}{\sqrt{1+z}-1}\right]^2, & z > 1 \end{cases}. \tag{96}$$

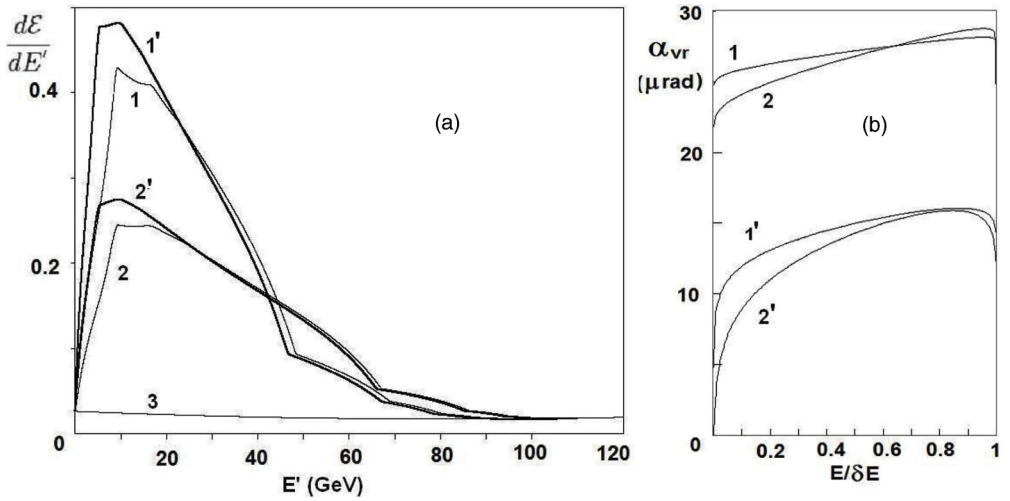

FIG. 6. (a) Averaged over transversal energy distributions of energy losses of positrons (1, 2) and electrons (1′, 2′). The conditions for calculations are $E_0 = 120$ GeV, crystal thickness is equal to 1 mm, bending radii are equal to 10 m (1, 1′) and 5 m (2, 2′). (b) The volume reflection angle for positrons (1, 2) and electrons (1′, 2′) as a function of the relative transversal energy. The functions are shown for one period.

IV. EXAMPLES OF CALCULATIONS

The aim of the examples presented here is the demonstration of various peculiarities of photon emission by light leptons moving in over-barrier states in bent planar electric fields. In parallel we will try to illustrate the possibilities to calculate the process with the help of different equations of the paper. Most of the calculations were carried out for the energy of particles equal to 120 GeV and the (110) planar fields of silicon single crystals, because the recent CERN experiment [11] was carried out for these conditions. Note that all calculations were performed at room temperature, for atomic form factors derived from x-ray experiments [18,21]. The comparison of calculations of volume reflection characteristics obtained on this basis with the corresponding experimental data [29,30] gives a measurably better result than with the use of the Moliere atomic form factors. Due to the squared dependence of the coherent radiation process on the interplanar potential (electric field), the correct choice of atomic form factors is important.

Figures 3 and 4 give an estimate of the mutual proximity of exact Eqs. (43)–(49) and approximate Eqs. (52)–(54). We see a rather good agreement, up to small enough κ parameters. In addition, Fig. 4 demonstrates that on a short distance the spectral energy losses are close to such losses in a straight single crystal. This fact supports results of the paper [10]. Besides, the use of Eqs. (52)–(54) [instead of Eqs. (43)–(49)] strongly simplified calculations [for example, see Eqs. (72)–(74), which take into account the multiphoton production].

Figure 5 illustrates the behavior of differential energy losses at various thicknesses of a single crystal. The calculations were made for the so-called symmetric orientation of a crystal. It means that the entrance and exit angles have the same absolute value but different signs [see Eqs. (19) and (20)]. The absolute value of the angle is equal to $\theta_c + z_0/(2R)$. For θ_c we take one half of the mean volume reflection angle (α_{vr}). We see that the form of the spectra is changed with thickness variations. This behavior differs from the similar one for straight single crystals, if the multiple scattering is not taken into account.

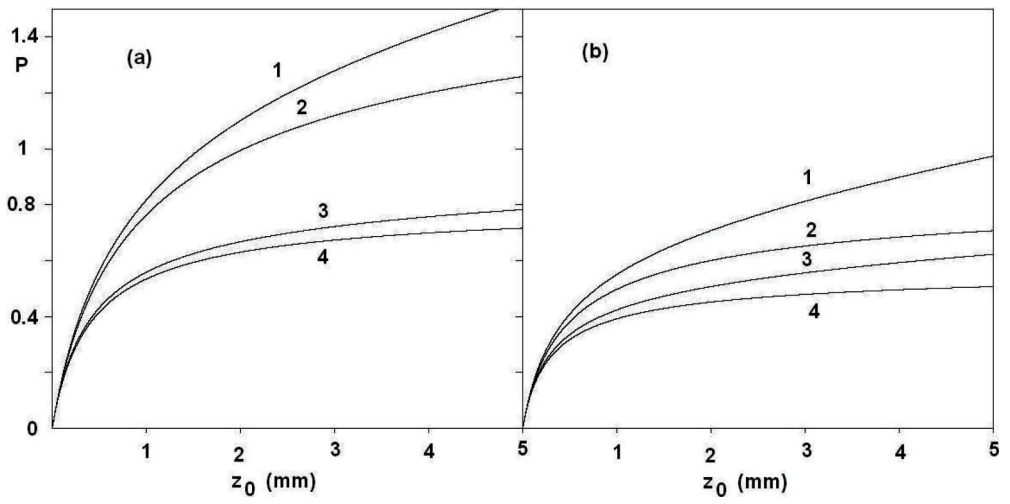

FIG. 7. Probabilities of photon radiation by positron as functions of a crystal thickness. For additional information see text.

Particles with the same entrance angle have different transversal energies [18] (defined by the initial coordinate x_0). According to Eq. (50), the correct value of radiation losses is a result of averaging over transversal energies [see Eq. (4)]. Figure 6 presents the calculations carried out in such a manner for a symmetric orientation. The choice of the entrance angle was made with the help of the relation $\theta_b = \langle\alpha_{vr}\rangle/2 + z_0/(2R)$. Due to the dependence of the volume reflection angle on the transversal energy, the outgoing particle beam gets some angle spread [see Eqs. (12) and (13)]. The absolute value of the exit angle for every particle can be found with the help of equation $\theta_e = z_0/R - \theta_b - \alpha_{vr}(E)$. Figure 6(b) illustrates the behavior of the $\alpha_{vr}(E)$ functions. Thus, these data are sufficient for finding the averaged spectra [see Eq. (50)]. As a result, we can conclude that it is not necessary to use the averaging procedure procedure for large enough bending radii (see Fig. 5, curve 3, and Fig. 6, curve 1, for comparison). The corresponding condition for bending radii is $R > E_0 d/U_0$, where U_0 is the interplanar potential barrier.

Comparing the corresponding results for electrons and positrons in Fig. 6 shows a small excess of losses for electrons in the soft part of the spectrum. It is easy to explain the smaller value of the mean volume reflection angle for electrons.

The form of the spectrum in Figs. 5 and 6 is clear. The first harmonic ($N = 1$) brings the main contribution in energy losses. In a straight single crystal the form of spectrum is defined by the θ angle. The photon spectrum begins from very small energies and reaches a maximal value which can be found from the relation $Gc\theta = \delta$ [see Eq. (56)]. The maximum of energy losses corresponds to the maximal photon energy (at fixed θ angle). Upon decreasing θ the maximal photon energy is also decreased. In a bent single crystal the θ angle is changed at the particle motion. Equations (19)–(20) show the area (of z or t variables) of stable motion in which $|\theta| < \alpha_{vr}/2$ is absent. This fact is equivalent to the suppression of the soft part of the spectrum, and we can write the condition for the photon energy which corresponds to the maximal value of energy losses: $Gc\langle\alpha_{vr}\rangle/2 = \delta$. From here we get

$$x_m = \frac{E_\gamma}{E_0} = \frac{D}{1+D}, \tag{97}$$

where $D = \lambda_c \gamma G \langle\alpha_{vr}\rangle$. One can obtain a similar estimate for the breaking of the spectral curve at high photon energies (from the condition $Gc\theta_b = \delta$) Taking into account that α_{vr} is

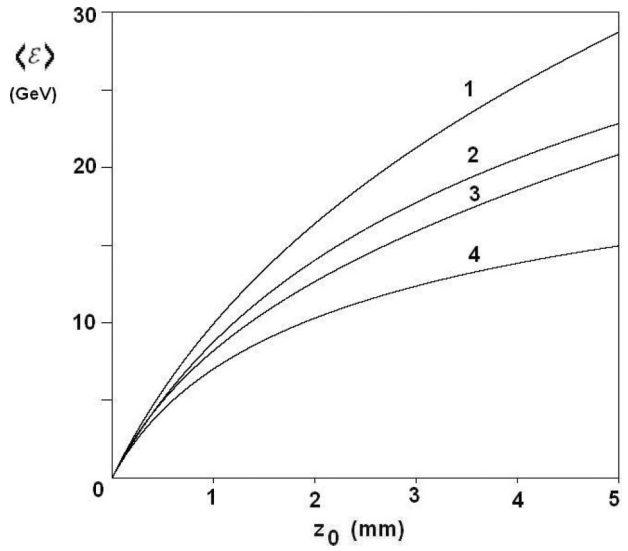

FIG. 8. Positron total energy losses as functions of a crystal thickness. The curves 2 and 4 correspond to pure coherent total energy losses. Bending radii are equal to 10 m (curves 1 and 2) and 5 m (curves 3 and 4).

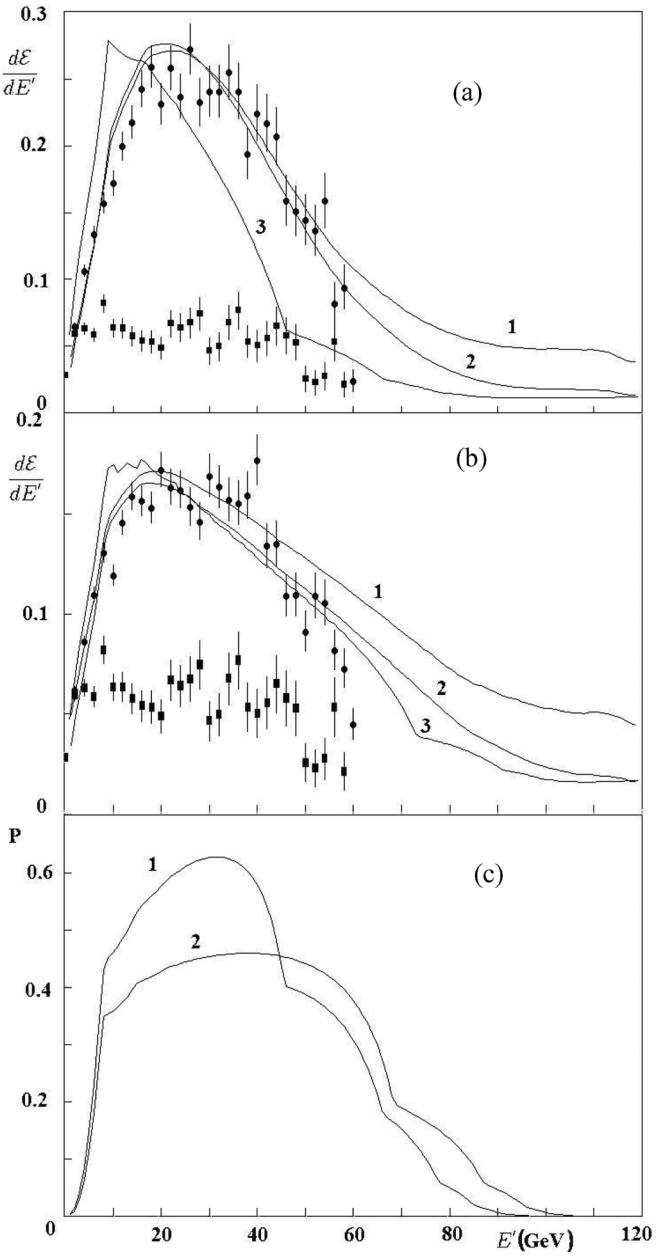

FIG. 9. Calculations of radiation energy losses [(a), (b)] and linear polarization (c) of 120 GeV positrons in the (110) plane of a silicon single crystal (2 mm of a thickness) as functions of energy. In panels (a) and (b) curves 1 present results of calculation of the total energy losses in the experiment (crystal + background), while the curves 2 correspond to a pure crystal. In panel (c) curves 1 and 2 present the linear polarization as functions of photon energy for bending radius 11 and 4.7 meters, respectively. For other explanations see text.

proportional to $\sqrt{E_0}$ (at large enough bending radii), we get that $x_m \approx D \sim \sqrt{E_0}$.

Equation (69) describes the probability of emission N_e/N_0 of a single photon as a function of a crystal thickness. This probability for a small crystal thickness has the form: $p_l(z_0) = n \int_0^{z_0} \sigma_\gamma(\epsilon, E_0, z) dz$ (in the linear approximation of the exponent in the equation). Figure 7 illustrates the behavior of these probabilities as a function of the thickness for two bending radii [10 m in Fig. 7(a) and 5m in Fig. 7(b)]. The curves 1 and 2 correspond to the linear probability $p_l(z_0)$ for two cases: (1) the cross section is a sum of the coherent and incoherent (at $\epsilon = 0.01 E_0$) cross sections (curve 1); (2) the cross section is a purely coherent one (curve 2) and $\epsilon = 0$. We employed Eqs. (72)–(74) for calculations. The curves 3 and 4 are the probabilities equal to $1 - \exp[p_l(z)]$ for cross sections as in the curves 1 and 2, correspondingly. One can see that for 10 m bending radius, both values p_l are about 1 at $z_0 \approx 2$ mm. It means, first, that the linear approximation does not work correctly at these thickness and, second, the probability of photon emission is close to 1 at a crystal thickness larger than 2 mm. Really, the curves 3 and 4 reach values of about 0.75 at 2 mm. For a crystal with 5 m bending radius the same situation takes place at a thickness about 4 mm.

Figure 8 illustrates the total energy losses of positrons as a function of the crystal thickness. We use Eqs. (66) and (67) for the calculation of the coherent contribution in the total losses.

Figure 9 presents the comparison of our calculations with the results of the recent CERN experiment [11]. The experiment was performed at a positron energy equal to 120 GeV. The silicon single crystal with the (110) orientation and 2 mm thickness was used in measurements, for two values of the bending radius (4.7 and 11 meters). Figure 9 illustrates the calculated spectra [Figs. 9(a) and 9(b) for bending radii 11 m and 4.7 m, respectively] and the degree of linear polarization [Fig. 9(c), the curves 1 and 2 for bending radii 11 m and 4.7 m, respectively]. The calculations are based on Eqs. (72)–(74) and so take into account the multiphoton production process.

The curves 1 and 2 correspond to two cases. The first case is the calculation for a pure crystal in the beam and the second one is for the sum of the crystal and the background from an additional substance in the beamline. Measurements (without crystal and with a nonoriented crystal) give a value equal to ≈0.7 for the ratio of energy losses. The circles and squares are the results of measurements for oriented and nonoriented positions. The curves 1 and 2 in Figs. 9(a) and 9(b) are the result of averaging over the angle divergence of the positron beam, which was ±50 and ±173 μrad relative to the central coming angle, respectively. Note that our calculation shows that averaged spectra are close to the spectra calculated for the central angle. This is also true for the polarization dependencies. The curves 3 [in Figs. 9(a) and 9(b)] are (multiplied by 0.65 and 0.85, respectively) the energy losses calculated with the help of Eq. (75) and hence do not take into account multiphoton production.

Besides, for a correct working of the method, the value ϵ should be defined correctly. Our choice of this value can be understood from the following simple arguments. In the experiment only energy losses larger than 2 GeV were fixed. Besides, the momentum spread of the positron beam was about 1 percent. It allows us to select ϵ equal to 1.2 GeV. Thus, we do not take into account the emission of low-energy photons. Results of calculations should be practically independent of the ϵ value. Really, for variations of ϵ in the range from 0.12 up to 1.2 GeV, the calculated spectra of energy losses are very close to one another. Our method is true for $\epsilon \ll 0.12$, but for the correctness of the use, the consideration of more than two-photon emission is needed. Besides, in the experiment the energy losses are determined mainly by the coherent part of the cross section, which has a finite value. Calculations

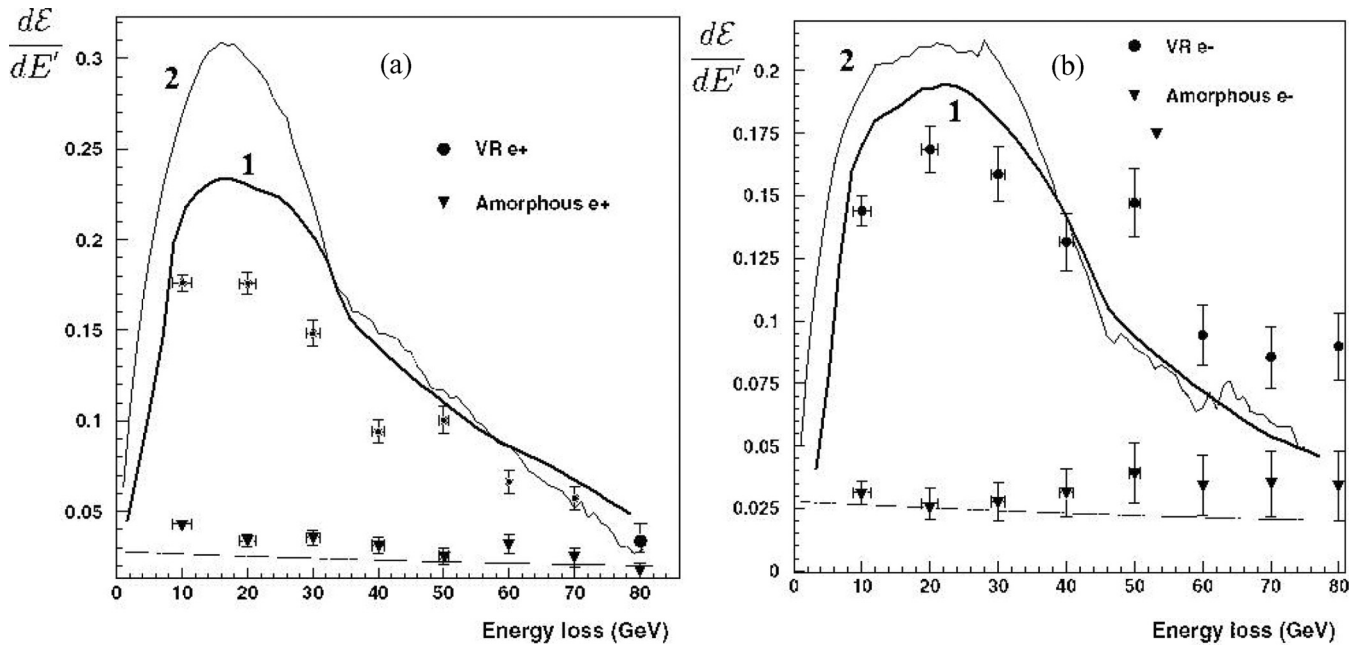

FIG. 10. Calculations of radiation energy losses of positrons (a) and electrons (b) in the (111) planes of silicon single crystals. The curves marked as 1 are new calculations, the curves 2 are previous ones [6]. Symbols are measurements.

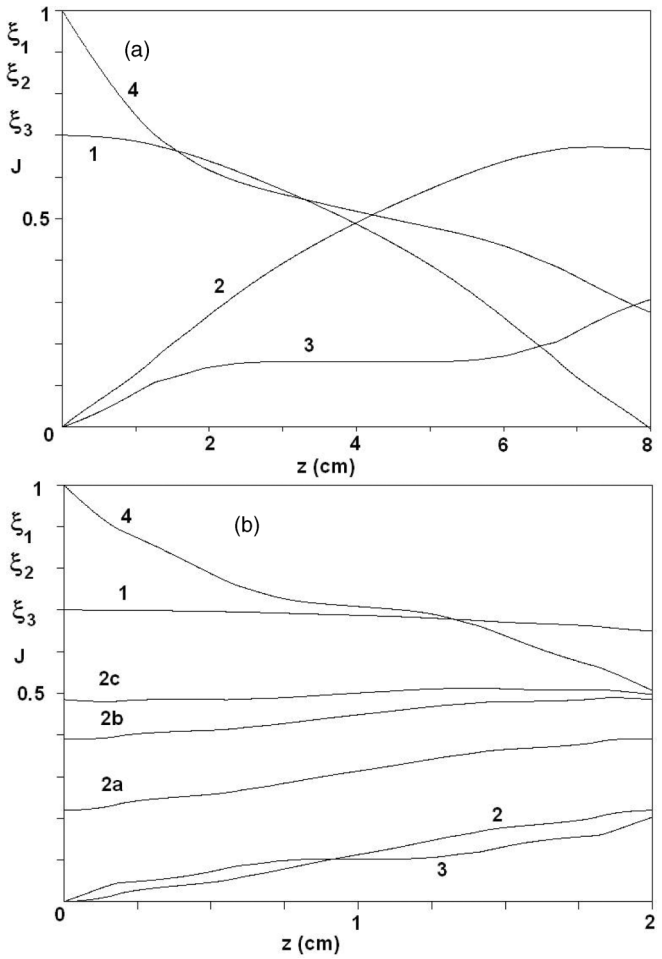

FIG. 11. Propagation of 1000 GeV photons through the (110) plane of a bent silicon single crystal. The curves 1–4 correspond to the Stokes parameters (ξ_1, ξ_2, ξ_3) and intensity (J), respectively. The bending radii and thicknesses are equal to 1000 m and 8 cm (a) and 100 m and 2 cm (b). The symmetric case of passage of beam is considered. The curves 2a, 2b, 2c demonstrate the transformation of the ξ_2 parameter by a sequence of several bent silicon crystals. The initial Stokes parameters are $\xi_1 = 0.7$, $\xi_2 = 0$, $\xi_3 = 0$.

with zero incoherent cross section (and $\epsilon = 0$) demonstrate insignificance and difference of results.

Additional amorphous material (besides the investigated single crystal) was present in the beamline and can give radiation energy losses of positrons which are not connected with the studied process. It is the usual situation in similar experiments. In such experiments, when the probabilities of interaction for both processes (i.e., the investigated and the background ones) are $\ll 1$, then these processes can be separated by a simple subtraction of the background one. In the case when the investigated process has large enough energy losses, this method does not work. Due to this fact we made approximate calculations of the influence of additional material on energy-losses spectra. As was mentioned above, the total differential cross section of the investigated process is the sum of the coherent $d\sigma_c$ and $d\sigma_a$ terms. We believe that the additional material may be taken into account by a corresponding increase of $d\sigma_a$.

We applied the method proposed here for the calculation of energy losses of 180 GeV positrons and electrons [6]. Figure 10 illustrates these calculations.

We made calculations of $e^{\pm}$ photoproduction probabilities with the help of Eq. (70) and the approximation Eq. (78) and found good agreement between them. One can find some illustrations of this process in Ref. [25]. Figure 11 demonstrates the propagation of 1000 GeV photons through a bent single crystal. Simple estimates show that a sizable variation of the Stokes parameters is possible only for high photon energies and for large enough crystal thicknesses. The figure shows also the possibility of using a sequence of several bent silicon crystals [31].

V. DISCUSSION

As mentioned above, the radiation in bent single crystals was considered in Refs. [12,13] In Ref. [12] the study of photon emission in bent crystals is based from the outset on the coherent bremsstrahlung mechanism. Because of this, a straight line particle motion (without any breaking at small angles) was assumed. The authors transform the relations for coherent bremsstrahlung into the cylindrical coordinate system with the use of the corresponding choice of the structure factors. The derived relations have a form similar to Eq. (55), with the introduced angle cutting parameter $\theta_{\min}$ which is equal to $\delta/(Gc)$ (in our notation). One can see that this parameter depends on the photon energy, and it is unrelated to the volume reflection angle. Unfortunately, in the paper specific calculations of the effect are not presented, but one can see from the equations that the characteristic maximum in the energy loss spectrum should be absent ($\theta_{\min} \to 0$ when $\omega_\gamma \to 0$).

In the papers [13,32,33] radiation energy losses are calculated for the case when the mean angle of volume reflection is equal to zero. This assumption is in conflict with experiments [29,30]. As a result of such consideration the spectra of energy losses (at orientations in the area of volume reflection) have a maximum at zero energy (see also Ref. [32]). According to Ref. [33] the linear polarization of the radiation is independent of the bending radius, and it has maximal value ($\approx$50%) in the soft part and tends to zero at the end of spectrum. Our calculations on the basis of Eq. (58) give another description (see Fig. 9). Note that some conclusions of Ref. [13] are in agreement with our description. The connection of the emission process in bent and unbent single crystals, the breaking of spectra at large energies are in agreement with our predictions.

It should be noted that multiple scattering of particles in a body of a crystal can change the probability of radiation if the scattering angle θ_m is close or exceeds the characteristic angle (which is equal to $1/\gamma$) of photon emission on the formation length. However, simple estimations performed for particle energies up to 200 GeV show that $\theta_m < 1/\gamma$ by several times. It means that multiple scattering does not disturb strongly photon emission on a short part of the particle trajectory. One can expect that the degree of perturbation depends on the initial particle energy and crystal thickness. The report [9] contains some results of the problem which was obtained by the Monte Carlo method. From here it follows that for a single crystal with

a thickness about 1 mm and an energy larger than 10 GeV the influence of multiple scattering is not strong.

Our calculations show that at a crystal thickness of about 1–3 mm the probability of photon radiation (see Fig. 7) is rather high (>0.7). A comparison of our simulations which take into account the multiphoton production with experimental data demonstrates good agreement (see Figs. 9 and 10). As shown in Fig. 9 there is the clear maximum of energy losses. The location of the maximum is shifted to higher photon energies than follows from Eq. (97). We explain this fact by a multiphoton production mechanism.

The propagation of high-energy photons in a straight single crystal (for orientations corresponding to coherent photoproduction) was studied, in particular, in Refs. [8,27,34–38]. In Refs. [39,40] the propagation was considered for the case of magneto pair production. As shown in Fig. 11 the initial linear polarization of the photon beam is transformed into a circular one. This phenomenon is due to interaction of the photon with the electron-positron field (vacuum polarization). There are two approaches to studying the phenomenon in crystals. The first one stands on the method of the electrodynamic of the continuous media and the second one stands on the methods of diagram calculations which allow one to obtain amplitudes of photon scattering at the interaction with crystal electric fields. In Ref. [41] the connection between these approaches was found: the relations between the permittivity (dielectric) tensor and the polarization tensor were established. The feature of the description of the propagation in bent single crystals is the coordinate (angle) dependence of the components of the permittivity tensor. The solution of this problem obtained in the paper has a rather common form and may be applied to similar ones. For example, in Refs. [42,43] variations of the Stokes parameters of high-energy photons going through a laser bunch was investigated for a constant photon density of bunch. Equations (88)–(91) give the solution for this case for variable density. Note that in the experiment [38,44], the indications on vacuum polarization in crystals were obtained. In principle, the bent single crystals may be used for investigations in this field.

We think that our consideration of electromagnetic processes my be extended to the axial case [45] of particle motion in bent single crystals. In the axial case we propose to use [instead Eq. (55)] the following equation:

$$\frac{d^2\mathcal{E}}{dE_q} = \frac{dI}{dE_q}(\theta_h(t),\theta_v(t))cdt, \tag{98}$$

where θ_h and θ_v are the angles which define the direction of motion in the local coordinate system xyz (see Fig. 1). Here, I is the well-known intensity of the coherent bremsstrahlung in a straight single crystal. Similar equations may be applied for an axial photoproduction process. The most promising result can be expected for the photon propagation, because the coefficient $a(z)$ [see Eq. (93)] should be 4–5 times larger than in the planar case [35].

In conclusion we can note that the description of electromagnetic processes in bent single crystals proposed here is in a good agreement with the existing experimental data and may be useful for different calculations in wide ranges of particle energies and crystal parameters (such as thickness, bending radius, sort of plane and others).

ACKNOWLEDGMENTS

The authors wish to thank Yu. A. Chesnokov and V. V. Tikhomirov for fruitful discussions. This work was partially supported by Russian Foundation for Basic Research Grant No. 11-02-90415.

[1] Yu. M. Ivanov *et al.*, Phys. Rev. Lett. **97**, 144801 (2006).
[2] W. Scandale *et al.*, Phys. Rev. Lett. **98**, 154801 (2007).
[3] V. Shiltsev *et al.*, in *Proceedings of 1st International Particle Accelerator Conference: IPAC'10*, Kyoto, Japan (2010), pp TUOAMH03.
[4] Yu. M. Ivanov *et al.*, JETP Lett. **84**, 372 (2006) [Pisma Zh. Eksp. Teor. Fiz. **84**, 445 (2006)].
[5] A. G. Afonin *et al.*, JETP Lett. **88**, 414 (2008).
[6] W. Scandale *et al.*, Phys. Rev. A **79**, 012903 (2009).
[7] Yu. A. Chesnokov, V. I. Kotov, V. A. Maisheev, and I. A. Yazynin, JINST **3**, P02005 (2008).
[8] V. N. Baier, V. M. Katkov, and V. M. Strakhovenko, *Electromagnetic Processes at High Energies in Oriented Single Crystals* (World Scientific, Singapore, 1998).
[9] V. A. Maisheev, *Report on CERN 4th Crystal Channeling Workshop* (2009) pp. 24–27, Geneve [http://indico.cern.ch/conferenceDisplay.py?confId=50840].
[10] V. A. Maisheev, Nuovo Cimento C **34**, 73 (2011).
[11] D. Lietti *et al.*, Nucl. Instrum. Methods Phys. Res. B **283**, 84 (2012).
[12] V. A. Arutunov, N. A. Kudryashov, V. M. Samsonov, and M. N. Strikhanov, Nucl. Phys. B **363**, 283 (1991).
[13] M. V. Bondarenco, Phys. Rev. A **82**, 042723 (2010).
[14] V. M. Biryukov and S. Bellucci, Nucl. Instrum. Meth. B **252**, 7 (2006).
[15] S. Bellucci *et al.*, Nucl. Instrum. Meth. B **252**, 3 (2006).
[16] S. Bellucci *et al.*, JETP Lett. **83**, 95 (2006) [Pisma Zh. Eksp. Teor. Fiz. **83**, 125 (2006)].
[17] S. Bellucci and V. M. Biryukov, Phys. Rev. ST Accel. Beams **10**, 013501 (2007).
[18] V. A. Maisheev, Phys. Rev. Spec. Top.–Accel. Beams **10**, 084701 (2007).
[19] V. M. Biryukov and S. Bellucci, Nucl. Instrum. Meth. B **266**, 235 (2008).
[20] A. I. Akhiezer and N. F. Shul'ga, *High-Energy Electrodynamics in Matter* (Gordon and Breach, Amsterdam, 1996).
[21] E. Bagli, V. Guidi, and V. A. Maisheev, Phys. Rev. E **81**, 026708 (2010).
[22] M. Ter-Mikaelyan, *High Energy Electromagnetic Processes in Condensed Media* (Wiley-Interscience, New York, 1972).
[23] H. Uberall, Phys. Rev. **103**, 1055 (1956).
[24] S. Bellucci and V. A. Maisheev, Phys. Rev. B **71**, 174105 (2005).
[25] Yu. A. Chesnokov, V. A. Maisheev, D. Bolognini, S. Hasan, M. Prest, and E. Vallazza, Phys. Rev. Spec. Top.–Accel. Beams **13**, 070706 (2010).

[26] V. A. Maisheev, V. L. Mikhalev, and A. M. Frolov, Sov. Phys. JETP **74**, 740 (1992).
[27] V. A. Maisheev, Phys. Lett. B **477**, 83 (2000).
[28] V. A. Maisheev, arXiv:hep-ph/0101191.
[29] W. Scandale *et al*., Phys. Rev. Lett. **101**, 234801 (2008).
[30] W. Scandale *et al*., Phys. Lett. B **681**, 233 (2009).
[31] W. Scandale *et al*., Phys. Rev. Lett. **102**, 084801 (2009).
[32] M. Bondarenco, J. Phys.: Conf. Ser. **236**, 012026 (2010).
[33] M. V. Bondarenco, Nuovo Cimento C **34**, 381 (2011).
[34] N. Cabibbo, G. Da Prato, G. De Franceschi, and U. Mosco, Phys. Rev. Lett. **9**, 435 (1962).
[35] V. A. Maisheev, arXiv:hep-ex/9904029.
[36] N. Z. Akopov, A. B. Apyan, and S. M. Darbinyan arXiv:hep-ex/0002041.
[37] V. M. Strakhovenko, Nucl. Instrum. Methods Phys. Res., Sect. B **173**, 37 (2001).
[38] A. Apyan *et al*., Phys. Rev. Spec. Top.–Accel. Beams **11**, 041001 (2008).
[39] V. G. Baryshevsky, V. V. Tikhomirov, and A. G. Shekhtman, Nucl. Phys. B **424**, 418 (1994).
[40] A. M. Frolov, V. A. Maisheev, and V. L. Mikhaljov, Nucl. Instrum. Methods Phys. Res., Sect. A **254**, 549 (1987).
[41] V. N. Baier and V. M. Katkov, Phys. Lett. A **286**, 299 (2001).
[42] G. L. Kotkin and V. G. Serbo, Phys. Lett. B **413**, 122 (1997).
[43] V. A. Maisheev, J. Exp. Theor. Phys. **85**, 1102 (1997); V. A. Maisheev, Zh. Eksp. Teor. Fiz. **112**, 2016 (1997).
[44] U. Uggerhoj, Rev. Mod. Phys. **77**, 1131 (2005).
[45] V. Tikhomirov, Phys. Lett. B **655**, 217 (2007).